Polymer 50 (2009) 2990–2998

Contents lists available at ScienceDirect

Polymer

journal homepage: www.elsevier.com/locate/polymer

Effects of spinodal decomposition on mechanical properties of a polyolefin blend from high to low strain rates

Liang Yang [a,b], Yanhua Niu [a,*], Howard Wang [c], Zhigang Wang [a,*]

[a] CAS Key Laboratory of Engineering Plastics, Beijing National Laboratory for Molecular Sciences, Institute of Chemistry, Chinese Academy of Sciences, Beijing 100190, PR China
[b] Graduate School, Chinese Academy of Sciences, Beijing 100049, PR China
[c] Department of Mechanical Engineering, State University of New York at Binghamton, Binghamton, NY 13902, USA

ARTICLE INFO

Article history:
Received 7 January 2009
Received in revised form
15 April 2009
Accepted 19 April 2009
Available online 3 May 2009

Keywords:
Polyethylene blends
Strain rate
Tensile properties

ABSTRACT

The effects of spinodal decomposition, a typical type of liquid–liquid phase separation (LLPS), on the mechanical properties of a pretreated statistical copolymer blend of poly(ethylene-*co*-hexene) (PEH) and poly(ethylene-*co*-butene) (PEB) were characterized by tensile testing under different strain rates. An important finding was that the strain rate and the crystallization temperature had to be considered as independent variables in analyzing the effects of spinodal decomposition on the tensile behaviors. At the high strain rate, the stress–strain curves kept irrespective of LLPS time, in which the interfacial relaxation between phase domains could not be detected, except the case crystallizing at 120 °C for 10 min. This was explained in terms of the distribution of the crystals elaborated by differential scanning calorimetry (DSC) results. However, when a relatively low strain rate was employed, a clear deterioration of tensile properties with LLPS proceeding was observed for the cases with low crystallization temperature because of its detection ability for large scale structural information, such as the phase boundary; unexpectedly, the effect of LLPS on the tensile properties was found to disappear in the high crystallization temperature cases which was due to the cooperative functions of the phase boundary and the internal structures of the phase domains. These abundant results provided a novel and indispensable instruction for the processing of polymer blends from the theoretical viewpoint.

1. Introduction

Polymers are known to exhibit strong time-dependent mechanical behaviors, as evidenced by strain rate dependent modulus, yield strength, post-yield behavior, and failure mechanisms [1–7]. A transition in the rate dependence of the yield behavior over a wide range of strain rate has been observed in poly(vinyl chloride) [8]. As the strain rate is increased, an additional stress is required to activate the secondary motions associated with local relaxation movements of small groups for the material to yield. On the other hand, the physical properties of polymer blends depend markedly on the supercrystalline morphology and phase boundary that result from crystallization termed as liquid–solid phase transition and potential liquid–liquid phase separation (LLPS) processes [9]. It is expected that detecting the molecular motions in different scales using different strain rate is as effective as detecting the effect of LLPS on tensile properties from the perspective of the phase boundary and the internal structures of phase domains.

The relationship between processing, possibly involving different deformation rate or injection speed, and phase morphology of polymer blends is a key issue to influence the application properties [10–12]. Up to date no well-advised experimental work which simulates the real processing or application for the miscible polymer blends has been reported [9,13–15]. It is only reported that a bi-continuous phase structure in polymer blends can provide polymers with nice mechanical properties such as high toughness, large extension, and excellent strain recovery [14,16]. Crystallization process affected by the LLPS is one of the main factors that determines the mechanical properties for miscible polyolefin blends, while the bi-continuous structure developed by the spinodal decomposition, a typical LLPS step also plays an important role on final tensile properties in this situation, because the mechanical properties of polymer blends are well known to be strongly affected by stress transfer between the phases in blends [17,18]. To understand mechanical properties, therefore, the above variables, crystal structure and phase boundary, have to be isolated and assessed individually. Methods of isolating these variables, by

* Corresponding authors. Tel.:/fax: +86 10 62558172.
E-mail addresses: yhniu@iccas.ac.cn (Y. Niu), zgwang@iccas.ac.cn (Z. Wang).

0032-3861/$ – see front matter © 2009 Elsevier Ltd. All rights reserved.
doi:10.1016/j.polymer.2009.04.031

control of crystallization conditions and strain rate, have to be applied to a poly(ethylene-*co*-hexene) (PEH) and poly(ethylene-*co*-butene) (PEB) copolymer blend, which can experience the spinodal decomposition during LLPS process. The redistribution of crystals occurred among phase domains with LLPS proceeding and its effect on tensile properties were discussed previously for the condition of crystallization at 120 °C for 10 min [9], however, we here in this study further raise the questions why the stress–strain curves treated under other crystallization conditions do not seem to be affected by LLPS at high strain rate and how strong effects the phase boundary can bring on the final properties if a different strain rate is applied.

In this work, the tensile properties of the H50 samples (Here the blend with 50% mass fraction of PEH is denoted as H50, the most representative composition for the PEH/PEB blends, which can experience the LLPS process through spinodal decomposition mechanism) treated with distinguishable LLPS times followed by different crystallization conditions at both above or below the crossover temperature (118 °C for H50) in the early or late stages were chosen to investigate. The evolution of co-continuous structures of H50 during LLPS process was primarily explored by scanning electron microscopy (SEM). Such experiments allow us to show that the phase boundary gradually sharpens with LLPS time for all the samples treated under each thermal condition. Accordingly, an obvious comparison is first set up between two experimental strain rates for the polymer blend systems, taking in mind the measurement ability on phase boundary information at low strain rate. We will also discuss the internal structures of phase domains, namely the crystal distribution, in the samples treated with four crystallization conditions *via* differential scanning calorimetry (DSC). Eight mechanical responses will be compositively delivered based on two competitive factors, the phase boundary and the internal structures of phase domains. Under a certain strain rate, it is the aim of this paper to establish the structure–property relationship by comparing the tensile properties under different thermal conditions. It is not our purpose here to develop particular procedures that yield the maximum tensile properties. This goal will be achieved eventually by comprehensive understanding on the competitive effects of phase boundary and phase domains that are formed in LLPS.

2. Experimental section

2.1. Materials

Statistical copolymers of ethylene and 1-hexene (PEH, M_w of 110 kg/mol, containing 2 mol% hexene comonomer) and of ethylene and 1-butene (PEB, M_w of 70 kg/mol, containing 15 mol% butene comonomer) were supplied by ExxonMobil Co. Ltd. Since they were synthesized with metallocene catalysts, the samples had relatively narrow polydispersity (~2) and uniform comonomer distributions. PEH was the only crystallizable component in the blend system throughout all the temperature conditions. Preparation of the blends followed the method described in a previous paper [19].

2.2. Thermal treatments and mechanical tensile tests

The films of the blend with thickness of about 0.5 mm for the mechanical tensile tests were obtained by compression molding at 160 °C. The films were enclosed into an airproof aluminum box for thermal treatments in oil baths before the mechanical tensile tests. Four distinct thermal treatment processes were applied to the films.

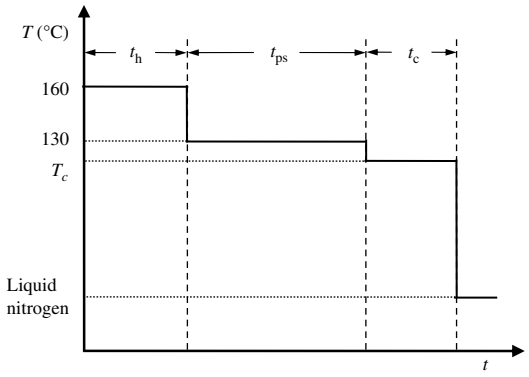

Fig. 1. Schematic illustration of the sample preparation processes. Annealing at 130 °C for different times and then isothermally crystallizing at $T_c = 100$ °C for 5 min or 10 h; or isothermally crystallizing at $T_c = 120$ °C for 10 min or 24 h. Here, t_h, t_{ps} and t_c denote melting time, LLPS time and isothermal crystallization time, respectively.

As shown in Fig. 1, the films in the aluminum box were firstly kept at 160 °C in the first oil bath for 10 min (denoted as t_h) to eliminate thermal history and were subsequently quenched to the designed phase separation temperature of 130 °C [19] in the second oil bath for different time (denoted as $t_{ps} = 0$, 2 and 20 h). Then, the films were quenched to a designed crystallization temperature T_c (100 or 120 °C) in the third oil bath for different time (denoted as $t_c = 5$ min or 10 h at 100 °C, named *Cond. A* or *Cond. B*, and $t_c = 10$ min or 24 h at 120 °C, named *Cond. C* or *Cond. D*). The temperature fluctuation during crystallization was less than ±0.1 °C. Finally, the films were quenched into liquid nitrogen. The thermal treatment processes for all the samples were identical to ensure comparability and accuracy for the tensile tests.

The dog-bone shape specimens with length of 14.0 mm, width of 6.0 mm and width of 2.3 mm at the neck position were die-cut from the above films. Mechanical tensile tests with an 8 mm initial gage length were performed at room temperature by using an Instron Universal Testing Machine. Two strain rates of 0.01 s^{-1} and 0.001 s^{-1} were chosen for the tests. Particular attention was paid to alignment of grips and specimen to achieve uniaxial elongation. In this report, we use engineering stress and nominal strain. Tensile modulus was determined from the slope of the secant line at 0.5% strain because of the inconspicuous linear region on the stress–strain curve [20]. Stress at 700% strain instead of the ultimate tensile properties is used for comparison among different conditions due to the error caused by sample geometry at the breaking point. The data reported here represent the averages of at least eight successful tensile tests.

2.3. Wide-angle X-ray diffraction (WAXD)

The values of crystallinity of the samples with thickness of about 0.5 mm cut from the films were obtained by WAXD measurements. The WAXD patterns in the diffraction angle range $2\theta = 5$–$35°$ were collected on a Philips X'pert pro diffractometer with a 3 kW ceramic tube as the X-ray source (Cu Kα) and an X'elerator detector. Because of the broadened diffraction contribution from the amorphous phase, the crystallinity, X_c, was evaluated by a peak deconvolution procedure, which had been described elsewhere [21]. The crystallinity values for the blends at different thermal treatment conditions are listed in Table 1.

2.4. Scanning electron microscopy (SEM)

In order to observe the bulk morphologies, the films were fractured in liquid nitrogen. All fractured film surfaces were etched at

Table 1
Crystallinity values for H50 with different thermal treatment conditions.

LLPS time (h)	*Cond. A*	*Cond. B*	*Cond. C*	*Cond. D*
0	0.24	0.23	0.22	0.23
2	0.24	0.23	0.22	0.23
20	0.24	0.24	0.22	0.23

room temperature for an appropriate time in 1% solution of potassium permanganate in a mixture of sulfuric acid and orthophosphoric acid, which preferentially etched the amorphous polymer in the crystals to make the crystal lamellae appear clearly. The fractured films were washed sequentially with hydrogen peroxide, distilled water and acetone, and then dried in a vacuum oven [22]. Before the SEM observation, the fractured film surfaces were coated with platinum.

2.5. Differential scanning calorimetry (DSC)

Calorimetric studies on the films were carried out in a TA Q200 differential scanning calorimeter (DSC). About 3.4 mg of pretreated samples were hermetically sealed in an aluminum pan for these measurements. Samples were heated from 20 to 160 °C at the rate of 10 °C/min.

2.6. Phase contrast optical microscopy (PCOM)

The blend samples were hot-pressed at 160 ± 2 °C to form films of ca. 20 μm and then quenched to room temperature. Phase contrast optical microscopy (PCOM) observation was carried out by using an Olympus (BX51) optical microscope connected to an Olympus (C-5050ZOOM) camera. A Linkam 350 hot stage was used to control the sample temperature. Thermal treatments for these samples were coordinate with the conditions described in Section 2.2 for preparation of the tensile testing samples. The characteristic lengths of spherulitic crystals and LLPS phase domains are obtained by 2-dimensional fast Fourier transform (2D-FFT) (images are shown at the top right corner as insets) of each corresponding optical micrograph in Fig. 5. The 1-dimensional scattering intensity profiles are extracted from the 2D-FFT images. The characteristic length is defined as $l = 2\pi/q_m$, where q_m is the scattering peak wave vector [23]. Note that only the results for the *Conds. C* and *D* cases are presented for further declaration.

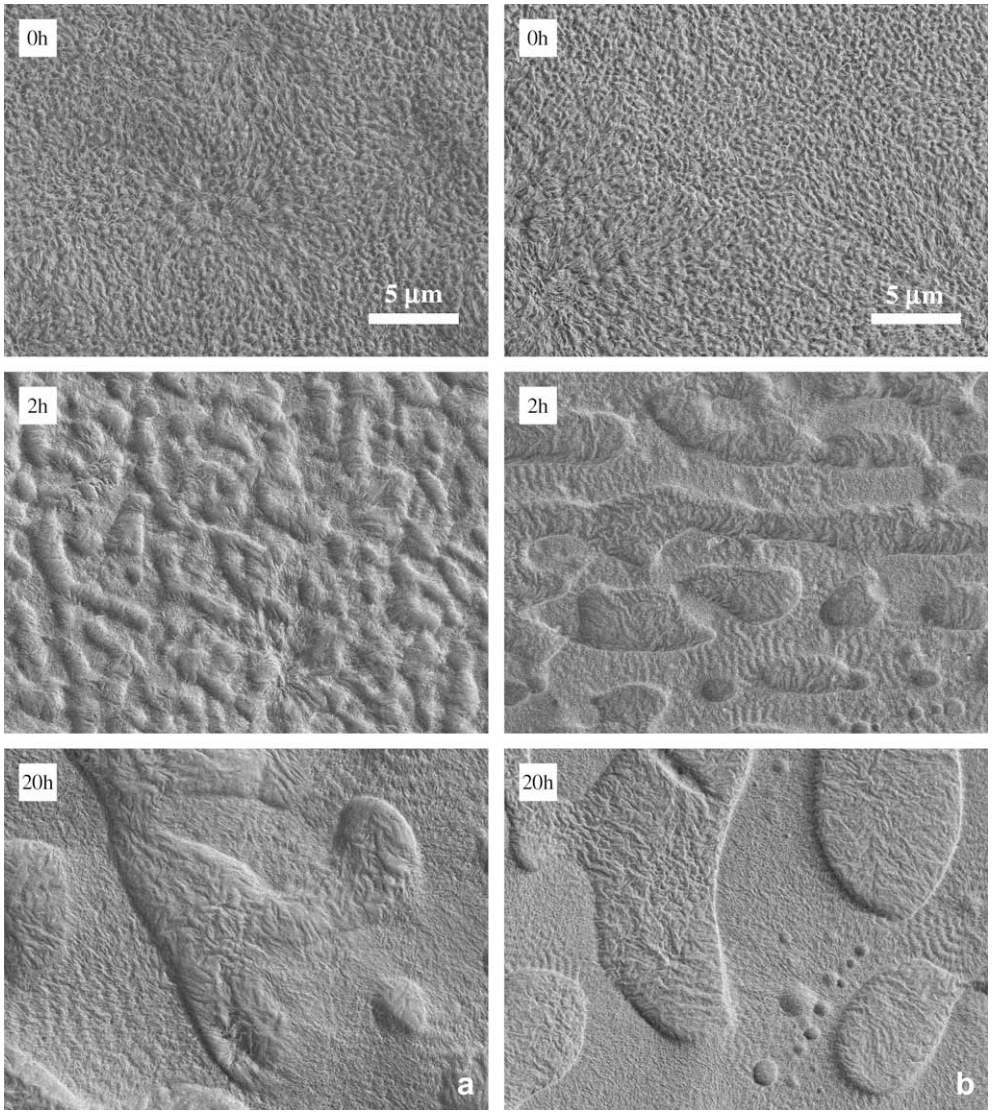

Fig. 2. SEM micrographs of cryo-fractured surfaces of H50 treated under (a) *Cond. A* (100 °C for 5 min), (b) *Cond. B* (100 °C for 10 h), (c) *Cond. C* (120 °C for 10 min) and (d) *Cond. D* (120 °C for 24 h). The scale bar in (a)–(c) corresponds to 5 μm and that in (d) corresponds to 10 μm.

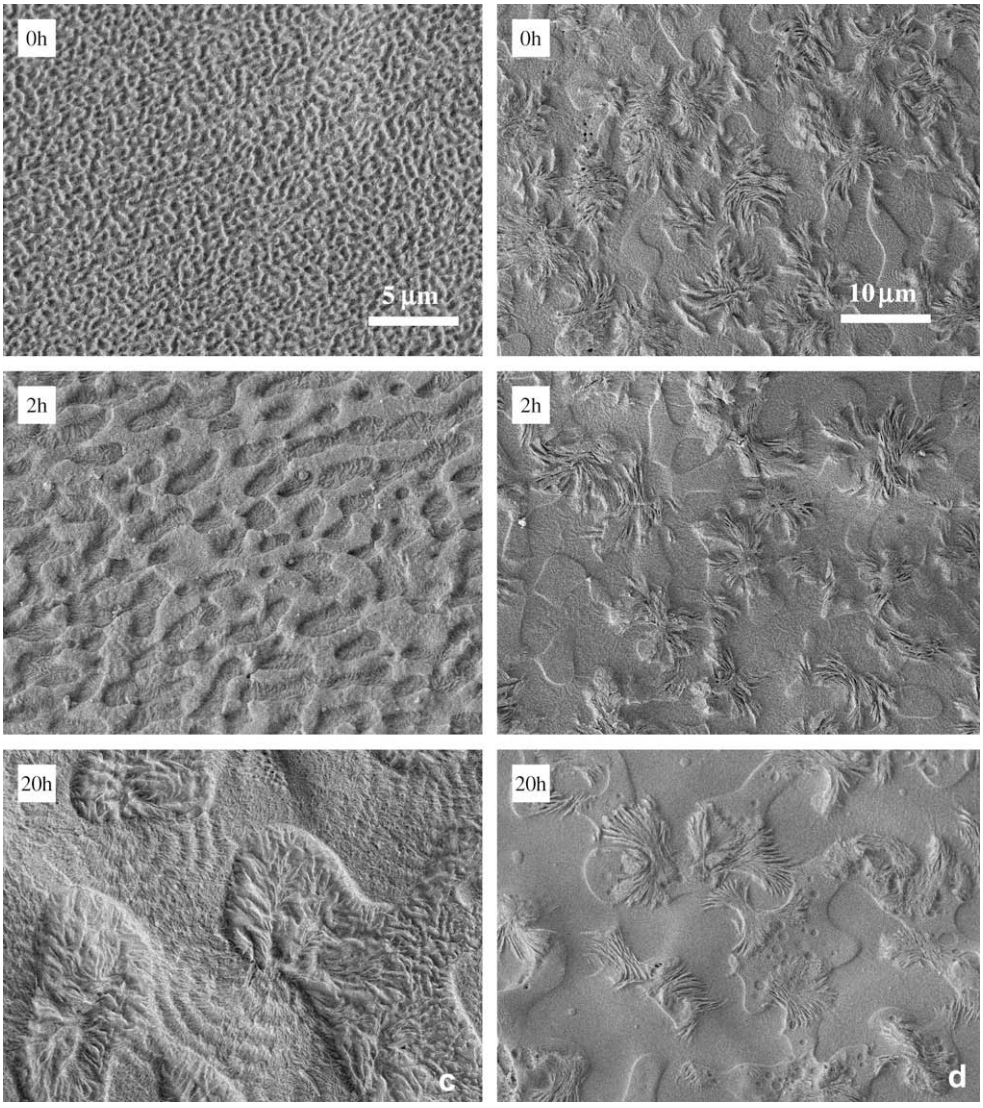

Fig. 2. (*continued*).

3. Results and discussion

3.1. Crystallinity of the samples at different thermal treatment conditions

It is well accepted that the crystallinity is proportional to the tensile properties of the sample [24,25]. In our case, as listed in Table 1, however, crystallinity values obtained from WAXD for H50 in three LLPS time cases (0, 2 or 20 h) keep approximately invariable for *Conds. A*,*B*,*C* and *D*. Meanwhile, considering the obvious effects of LLPS on the tensile properties for the eight mechanical consequences shown in Fig. 4, there must exist some other structural factors resulted from LLPS, besides the crystallization effect, which determine the final properties. Next, we will pay our attention on the phase morphologies together with the detection ability to the phase boundary under different strain rates and the origin of uneven crystal distributions among phase domains.

3.2. Phase morphologies at different thermal conditions

SEM was employed to examine the phase morphologies of PEH/PEB blends in this study. From the SEM micrographs of H50 treated with *Conds. A*,*B*,*C* or *D* (see Fig. 2), it is worth noting that more clear co-continuous structure inside the bulk polymer formed through the spinodal decomposition mechanism can be directly identified and the sizes of dispersed phase increase gradually with increasing phase separation time, indicating thermodynamically spontaneous tendency towards the equilibrium state. Such an increase in coarseness must be associated with increase in the sizes of the PEB-rich phase that is extracted during etching. It is reported [26] that, for the immiscible polymer blends, the smooth phase boundary cannot retard the slippage of two phases under deformation at a certain crosshead speed, and the mechanical properties become poor. On the contrary, the partially miscible polymer blends in our study with the rough and diffuse phase boundary as shown in the SEM micrographs and the rather low interfacial tension ranging from 0.5 to 0.38 mN/m [27] should have sturdy morphologies normally [28–31] and deform cooperatively between two phases, and the dependence of tensile properties on phase domain morphology strongly relates to the applied strain rate. In general, the strain rate in tensile test or the frequency in rheological test has detection limits according to the phase boundary situation, which might be determinate for any particular thermal treatment case and will be confirmed in Sections 3.4 and 3.5.

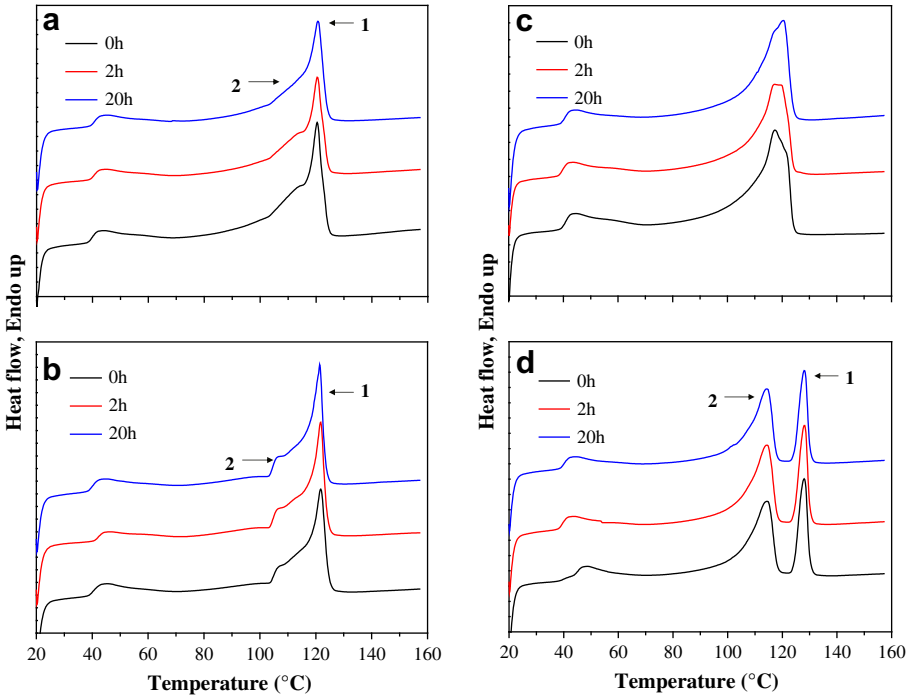

Fig. 3. Heating scan curves of H50 treated under (a) *Cond. A* (100 °C for 5 min), (b) *Cond. B* (100 °C for 10 h), (c) *Cond. C* (120 °C for 10 min) and (d) *Cond. D* (120 °C for 24 h).

3.3. Crystal distribution probed by differential scanning calorimetry

Although SEM can tell the situation of phase boundary as illustrated in Fig. 2, the internal structures of phase domains or the distribution of crystals must be further examined by using other techniques, for example, differential scanning calorimetry (DSC). Fig. 3 shows the heating scan curves of H50 treated under *Conds. A,B,C* and *D*. We can easily observe three endothermic peaks (including one shoulder) in Fig. 3a,b and d with the higher temperature melting peak (endotherm 1) corresponding to melting of thicker lamellae formed during isothermal crystallization at 100 °C or 120 °C and the lower temperature melting peak (endotherm 2) corresponding to melting of thinner lamellae formed during the quenching step. The minor endothermic peak locating at approximate 45 °C is related to melting of small crystals formed during the sample annealing at room temperature [32]. Similar observation has also been reported [33,34]. The almost unchanged peak shape and position among the three heating scan curves in Fig. 3a,b and d for *Conds. A, B* and *D* indicate that the distribution of crystals [35] does not show measurable differences with different LLPS time for each condition. On the contrary, heating scan curves of H50 treated under *Cond. C* exhibit notable differences regarding to the higher temperature endothermic peak among the three LLPS time cases. The higher temperature endothermic peak area increases with prolonged LLPS time, indicating that the proportion of crystals with thicker lamellae increases as LLPS time increases, in other words, lamellar crystals have more uneven distribution with longer LLPS time for *Cond. C*.

We attempt to explain the significant differences among the different DSC results. For *Conds. A* and *B*, the readily formed phase separation domains can be locked-in upon crystallization beginning at 100 °C [36,37]. Due to fast crystallization, polymer chains rearrange dramatically, which seems difficult to invoke a noticeable redistribution of crystals for a long LLPS time case as opposite to the situation in *Cond. C* [9]. This phenomenon named as a diffusion-controlled process has been elaborated in the literatures, which indicates that the crystals distribute evenly for *Conds. A* and *B* with different LLPS times [37]. While for the samples isothermally crystallized at 120 °C, crystal growth is much slower than that at 100 °C and enough time is provided for the growing front of a given PEH lamella to extract PEH chains from the PEB-rich phase domains [9]. Recalling the difference in the dynamic process of the two crystallization temperature cases, the crystal redistribution could only happen for the case at higher crystallization temperature, like *Cond. C* in our study, which results from the crystal growths through the phase-separated domains. The situation of *Cond. D* is considered as an exclusive case, which will be separately discussed in Section 3.6.

3.4. Mechanical properties at high strain rate

From the previous rheological testing, the critical frequency ω_c corresponding to the onset of thermorheological complexity marked in Fig. 2 of Ref. [19] is about 0.1 rad/s, which suggests that the additional long relaxation of the interface emerges at frequency lower than 0.1 rad/s. The particular frequency of rheological test can be converted to corresponding average strain rate by using Eq. (1) as follows:

$$\dot{\varepsilon} = \text{strain/time} = 4\varepsilon_0\omega \tag{1}$$

where ε_0 is the maximum strain amplitude achieved at one quarter of the loading cycle [8], yielding a critical strain rate of $\dot{\varepsilon}_c = 0.003\ s^{-1}$. It is reasonable to expect that the boundary effect, particularly the change of interfacial tension with LLPS time, gradually evolves from the undetectable state to the detectable state for the mechanical behavior when tensile strain rate is lowered from $0.01\ s^{-1}$ to $0.001\ s^{-1}$ ($0.001\ s^{-1} < \dot{\varepsilon}_c = 0.003\ s^{-1} < 0.01\ s^{-1}$).

The strain rate dependence of the effect of co-continuous structure on the tensile properties was investigated for H50 as

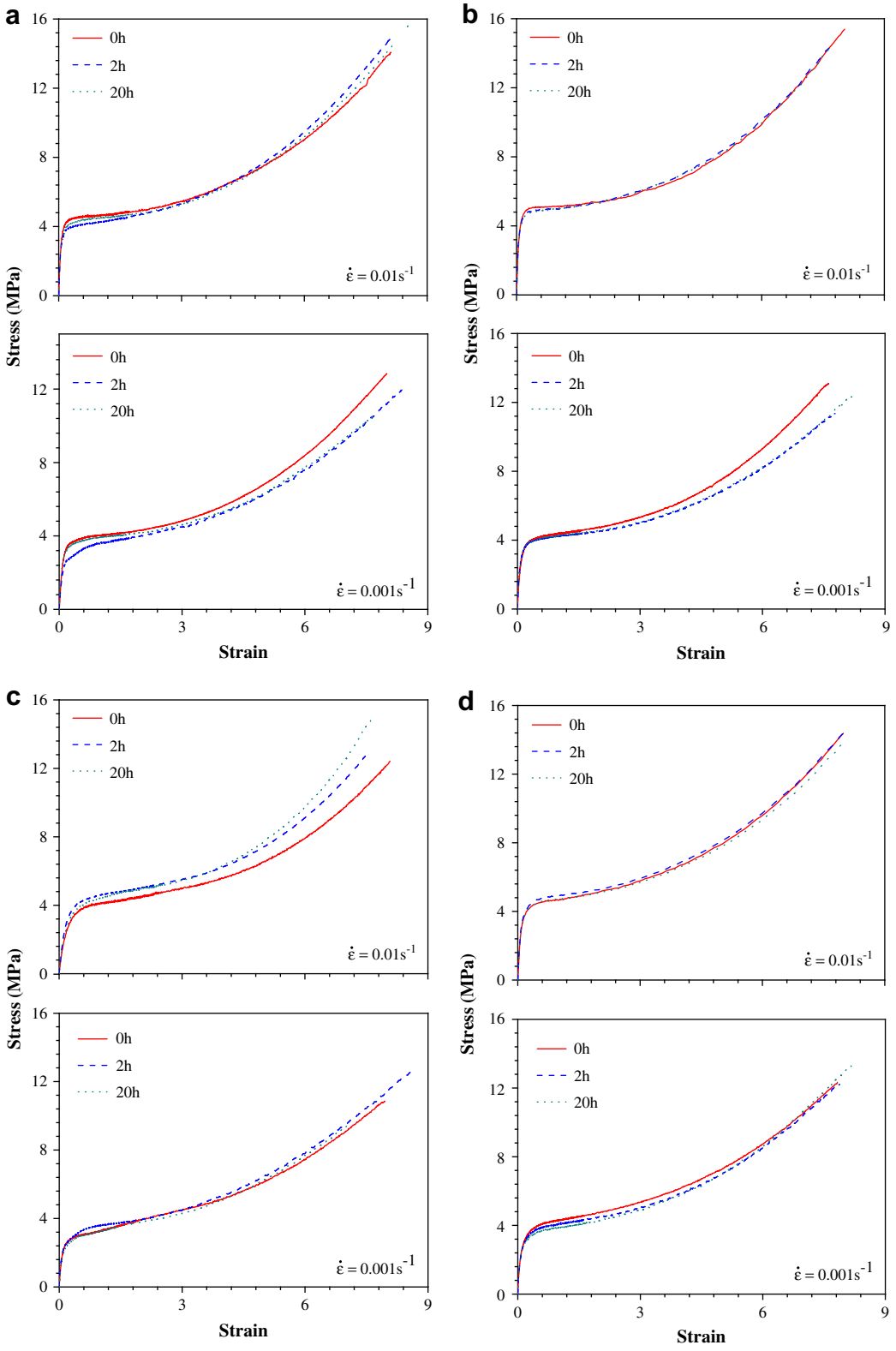

Fig. 4. Typical stress–strain curves of H50 treated under (a) *Cond. A* (100 °C for 5 min), (b) *Cond. B* (100 °C for 10 h), (c) *Cond. C* (120 °C for 10 min) and (d) *Cond. D* (120 °C for 24 h). The samples were extended at the strain rate of 0.001 s^{-1} and 0.01 s^{-1}, respectively, as denoted in the figures.

a representative example. Fig. 4 presents the stress–strain curves of H50 treated under *Conds. A,B,C* and *D* at strain rates of 0.01 s^{-1} and 0.001 s^{-1} (0.01 s^{-1} for the upper three curves and 0.001 s^{-1} for the lower three ones).

When the strain rate is higher than 0.003 s^{-1}, namely 0.01 s^{-1}, the effect of LLPS on tensile properties is simplified into the effect of the internal structures of phase domains on the final properties because the phase boundary information or the interfacial

relaxation between phase domains cannot be detected at this high strain rate. As shown in Fig. 4a–d (the upper three curves in each figure), rules of independence of tensile properties on LLPS time are quite uniform for *Conds. A,B* and *D*, however, some slight but obvious differences must be noted for the samples at *Cond. C* which were isothermally crystallized at 120 °C for 10 min, for that the reasons have been provided in our previous study [9].

For *Conds. A* and *B*, where the crystallization temperature is well below the crossover temperature, such as 100 °C, the stress–strain curves do not seem to vary with LLPS time for both short (5 min) or long (10 h) crystallization times. As mentioned above, the phase boundary effects on the mechanical properties can be negligible at high strain rate, thus we only need to consider the internal structure effects of the crystals herein. According to the results in Section 3.3, at relatively low crystallization temperature, i.e. 100 °C in our case, crystals distribute evenly in the samples with different LLPS times. Therefore, the effect of phase separation on crystallization is largely weakened and hence the tensile properties of the blends seem to be independent of the prior occurred liquid–liquid phase separation in these cases.

In order to slow down the crystallization rate and magnify the function of LLPS, the relatively higher crystallization temperature

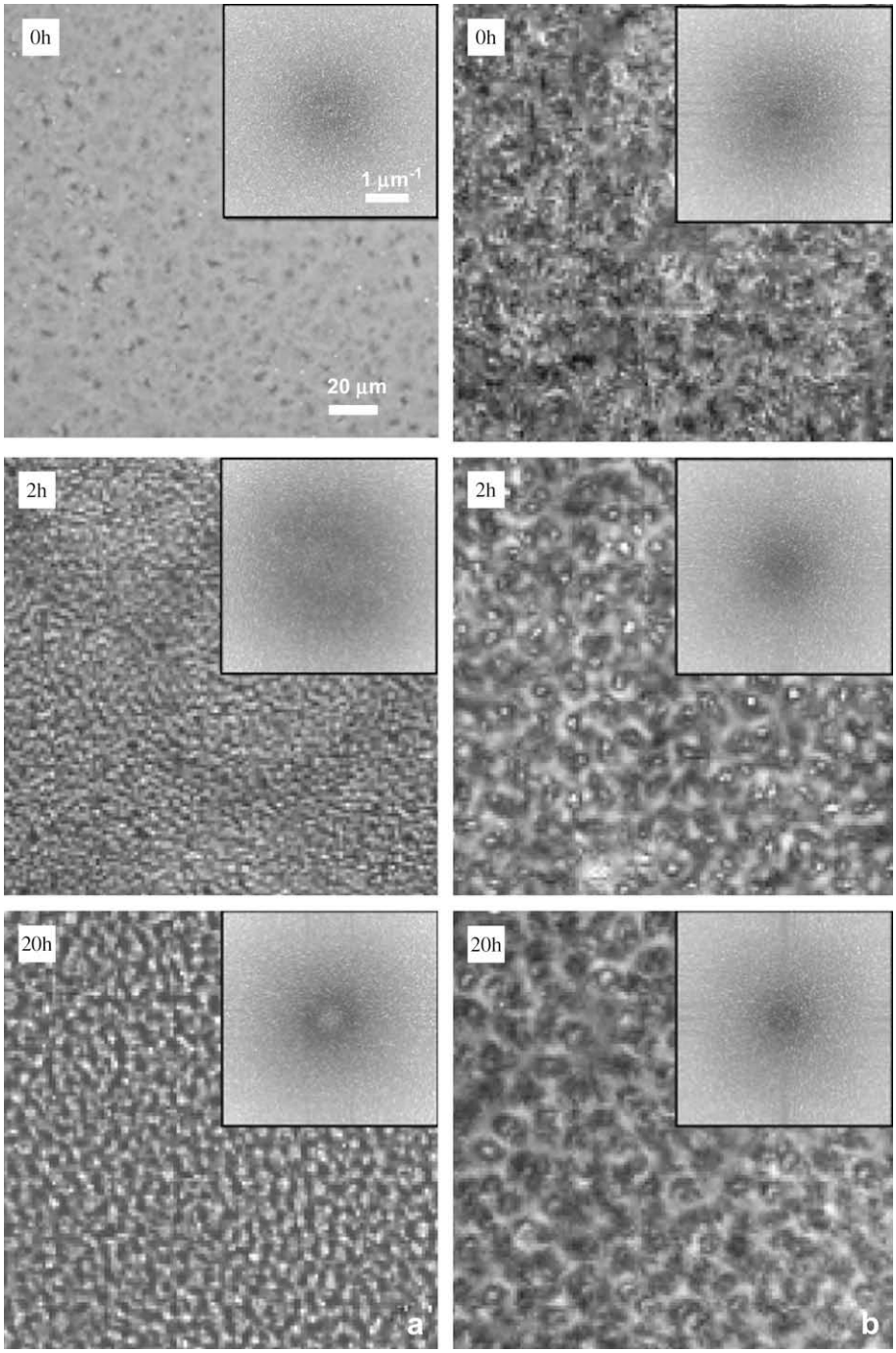

Fig. 5. Phase contrast optical micrographs of H50 for the cases of (a) *Cond. C* and (b) *Cond. D*. Scale bars in (a) and (b) correspond to 20 μm for all the optical micrographs. Insets show the corresponding 2D-FFT images, in which the scale bar represents 1 μm^{-1} for all the FFT images.

of 120 °C was selected, which is above the crossover temperature of 118 °C. Learning from the discussion in Section 3.3, we know that the crystals redistribute for the *Cond. C* case with longer LLPS time [9]. Consequently, the enhanced effect of the variation of the phase internal structures on the mechanical properties is able to present in *Cond. C*, but disappears in *Conds. A* and *B*. The results for the *Cond. D* case will be exclusively discussed in Section 3.6.

3.5. Mechanical properties at low strain rate

Since the effects of LLPS on tensile properties originate from multiple factors, the phase boundary effect can be detected when the strain rate is reduced from $0.01\,s^{-1}$ to $0.001\,s^{-1}$ (lower than $\dot{\varepsilon}_c = 0.003\,s^{-1}$). Different thermal treatment conditions cannot fully account for the variations in tensile properties. Consequently, the following experimental results in this section are explained on the basis of the competitive relations between phase boundary and internal structures in phase domains.

For the *Conds. A* and *B* cases, as shown in Fig. 4a and b (the lower three curves), the linear region of the stress–strain curve maintains invariable with LLPS time, while the stress at large strain of 700% deceases prominently by about 15% from 0 h to 2 h and 20 h LLPS time cases. With the notion that the large strain tensile property, i.e. stress at 700% strain, is undeniably more sensitive to detect the effect of the co-continuous morphology than the small strain tensile property [38,39], we can basically explain the results as follows. At low temperature (100 °C), the function of internal structures of phase domains is totally suppressed as discussed in Section 3.3, which still cannot be exhibited at low strain rate, and the interfacial tension becomes dominant in determining the final mechanical properties in this situation. Apart from the coarsening evolution of the bi-continuous interconnected morphology during the concentration fluctuations of spinodal decomposition, the amount of interphase decreases and the phase boundary turns to sharpen from 0 h to 2 h LLPS times (Fig. 2a and b). Concomitantly, the interfacial tension between the two phase domains decreases, which can be detected under the low tensile strain rate of $0.001\,s^{-1}$ [17]. Obviously, the tensile properties deteriorate due to the weakened interfacial tension with long LLPS time.

While for the *Cond. C* case, as shown in the lower three curves of Fig. 4c, the stress–strain curves cannot be differentiated for the different LLPS time cases. In contrast to 100 °C in *Conds. A* and *B*, the favorable influence of internal phase structures should not be neglected at the high crystallization temperature (120 °C). In our previous work, it is demonstrated that although the average structure parameters, like crystallinity or entanglement density, do not change in the global bulk sample, the local assembly of more crystallizable component is prone to enhance the critical stress needed to deform the sample in both the low and high strain ranges [9]. However, in the present study with the low strain rate, the positive effect of internal phase structures on the tensile properties seems to be counteracted by the negative effect of phase boundary somehow or even in total. Consequently, the whole effects of LLPS on the tensile behavior disappear in this case. Then, it would be easy to understand why the stress–strain curves with different LLPS times in Fig. 4c (the lower three curves) can be delineated into one curve.

3.6. Further analysis on the Cond. D case

Based on the above discussion, one might normally expect that increasing the LLPS time would enhance the tensile properties of the samples treated under *Cond. D* at the high strain rate, similar to that in *Cond. C*. However, our experimental data show a surprising result. As shown in Fig. 4d, the stress–strain curves superpose into one master curve irrespective of LLPS time at both the high and low strain rates. The key factor that leads to this exclusive result is the long crystallization time of 24 h for *Cond. D*. We cannot rule out the truth that LLPS process keeps proceeding at 120 °C within 24 h due to the high crystallization temperature. Therefore, the relative dimensions of the spherulitic crystals and the bi-continuous structure might be quite different from the other three conditions.

Since the morphologies induced by the kinetic competition between crystallization and LLPS at low crystallization temperature, like 100 °C in our study (*Conds. A* and *B*), are similar to that reported by Tanaka [40], our attention here only focuses on the situations of *Conds. C* and *D* at high crystallization temperature. Fig. 5 shows the phase contrast optical micrographs of H50 treated under *Cond. C* (see Fig. 5a) and *Cond. D* (see Fig. 5b). The interconnected bi-continuous morphologies coupling with spherulitic crystals are observed, while the major difference lies in their relative dimensions. After the fast Fourier transform, the 2D-FFT scattering intensity patterns can be radially averaged to yield the 1-dimensional scattering intensity profiles as shown in Fig. 6. One can see from Fig. 6a that two scattering peaks show up with one at low q corresponding to the characteristic length of spherulitic crystals and the other one at high q corresponding to the characteristic length of LLPS phase domains [23], which indicates that the sizes of the former are larger than the latter for *Cond. C*. On the contrary, only one scattering peak at low q remains constant in position but becomes more diffused with LLPS proceeding as seen in Fig. 6b,

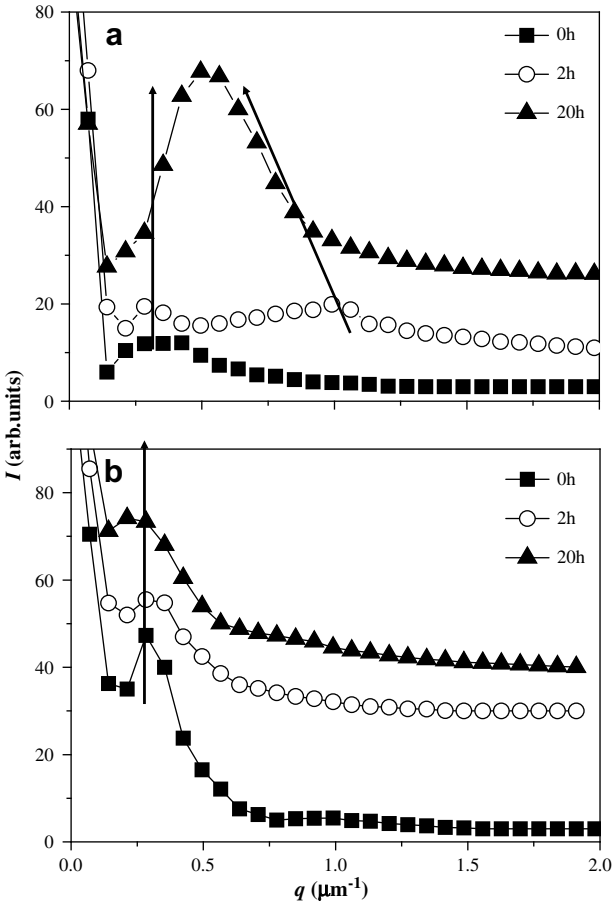

Fig. 6. 1-Dimensional scattering intensity profiles of H50 from the 2D-FFT images in Fig. 5 insets for the cases of (a) *Cond. C* and (b) *Cond. D*.

which appears that the scattering peak from LLPS phase domains vanishes, and in fact, the characteristic lengths of spherulitic crystals and LLPS phase domains become actually comparable for *Cond. D*.

The above results can be explained in terms of different isothermal crystallization times. For the *Cond. C* case, the crystallization happening during the quenching step cannot be neglected due to the short isothermal crystallization time (10 min). Substantially, the crystallization process in *Cond. C* with a fast crystallization rate during the quenching step is similar to the situations in *Conds. A* and *B*. Hence, the characteristic lengths of spherulitic crystals are larger than the bi-continuous phase domains dimensions for *Cond. C* which results from the crystal growths through the phase domains. However, the scale of the macroscopic phase separation is larger than the diameter of the spherulite when the LLPS process is faster than the crystallization process with long enough time [37,40], for example, in the *Cond. D* case. For the *Cond. D* case, the scale of the phase domains is not smaller than the spherulitic sizes in the final sample, which can lead to two results. One is that the distribution of the spherulites remains almost the same for the different LLPS times, because the LLPS process has reached the very late stage in *Cond. D* for all three LLPS times due to the large quenching depth of LLPS at 120 °C. Hence, no incentive for the variation of the uneven distribution of crystals exists (see Fig. 3d), so the increasing effect of internal structures of phase domains is nullified. The other result is that the phase boundary approximately locates in the amorphous region, which indicates that the sharpening of the phase boundary could hardly affect the final properties due to the similar mechanical properties between the amorphous parts of PEH and PEB. Combining the above two results, the LLPS does not show any influences on the tensile properties at both high and low strain rates for the exclusive *Cond. D* case.

4. Conclusions

In attempting to summarize our results, it should be recognized that the partially miscible polymer blends of polyethylene type consist of bi-continuous structure where three-dimensional spherulites disperse randomly. All the variations in the crystal distribution and the interconnected phase morphology of the blends play important roles to determine the mechanical behaviors.

In conclusion, phase boundary sharpening caused by LLPS always leads to detrimental tensile properties, while the redistribution of crystals happening inside phase domains enhances the tensile properties. These two competitive factors can be presented by selecting appropriate strain rate and crystallization temperature, respectively. More specifically, at a relatively high strain rate the effect of the proceeding phase separation on the total crystallinity and final mechanical properties of the blends becomes less significant for the low crystallization temperature cases, regardless of the isothermal crystallization time, since the effect of interfacial tension is suppressed. However, the function of prior occurred phase separation maintains obvious for the short crystallization time case at high temperature, showing an increasing effect upon the tensile properties as LLPS proceeds. When a low strain rate is applied, the tensile properties developed at low crystallization temperature weaken with increasing LLPS time because the phase boundary sharpening governs the tensile behaviors. In the opposite case, competitive effects of phase boundary and internal phase structures at high crystallization temperature for *Cond. C* are found to cooperatively affect the mechanical properties of the PEH/PEB blend and the final consequence is counteracted. While for the special case of *Cond. D*, LLPS proceeding does not affect the tensile properties because the phase domains almost comprise the spherulitic crystals at both the high and low strain rates. Our discovery of the strain rate dependent effects of spinodal decomposition (LLPS) on the mechanical properties of polyolefin blends reveals a simple and effective way to adjust the mechanical properties of the semicrystalline polymer blends and to estimate the practical properties in a real certain circumstance.

Acknowledgments

The authors acknowledge the financial support from National Science Foundation of China with Grant No. 20674092 and 50573088 and National Science Foundation of China with Grant No. 10590355 for the State Key Project on Evolution of Structure and Morphology during Polymer Processing. The authors would like to thank Prof. Erqiang Chen for the availability of the X-ray diffraction facility at the Peking University. HW acknowledges the support by the National Science Foundation (USA) under Grant No. DMR-0711013.

References

[1] Drozdov AD, Christiansen JD. Polymer 2003;44:1211.
[2] Grein C, Plummer CJG, Germain Y, Kausch HH, Beguelin P. Polym Eng Sci 2003;43:223.
[3] Hiss R, Hobeika S, Lynn C, Strobl G. Macromolecules 1999;32:4390.
[4] Scogna RC, Register RA. Polymer 2008;49:992.
[5] Soong SY, Cohen RE, Boyce MC, Chen W. Polymer 2008;49:1440.
[6] Termonia Y, Meakin P, Smith P. Macromolecules 1986;19:154.
[7] Kolarik J, Pegoretti A. Polymer 2006;47:346.
[8] Soong SY, Cohen RE, Boyce MC, Mulliken AD. Macromolecules 2006;39:2900.
[9] Yang L, Niu YH, Wang H, Wang ZG. Polymer 2009;50:627.
[10] I'Abee R, Goossens H, van Duin M. Polymer 2008;49:2288.
[11] Omonov TS, Harrats C, Moldenaers P, Groeninckx G. Polymer 2007;48:5917.
[12] Tang XG, Yang W, Shan GF, Yang MB, Xie BH, Fu Q. Polymer 2007;48:7404.
[13] Bucknall CB, Partridge IK. Polymer 1983;24:639.
[14] GirardReydet E, Vicard V, Pascault JP, Sautereau H. J Appl Polym Sci 1997;65:2433.
[15] Williams RJJ, Rozenberg BA, Pascault JP. Polym Anal Polym Phys 1997;128:95.
[16] Quintens D, Groeninckx G, Guest M, Aerts L. Polym Eng Sci 1990;30:1474.
[17] Murata K, Anazawa T. Polymer 2002;43:6575.
[18] Paul DR, Newman S. Polymer blends. New York: Academic Press; 1978.
[19] Niu YH, Wang ZG. Macromolecules 2006;39:4175.
[20] Wang HP, Khariwala DU, Cheung W, Chum SP, Hiltner A, Baer E. Macromolecules 2007;40:2852.
[21] Wang ZG, Hsiao BS, Sirota EB, Agarwal P, Srinivas S. Macromolecules 2000;33:978.
[22] Saengsuwan S, Bualek-Limcharoen S, Mitchell GR, Olley RH. Polymer 2003;44:3407.
[23] Shimizu K, Wang H, Matsuba G, Wang ZG, Kim H, Peng WQ, et al. Polymer 2007;48:4226.
[24] Crist B, Fisher CJ, Howard PR. Macromolecules 1989;22:1709.
[25] Peacock AJ, Mandelkern L. J Polym Sci Part B Polym Phys 1990;28:1917.
[26] Pang YY, Dong X, Zhao Y, Han CC, Wang DJ. Polymer 2007;48:6395.
[27] Niu YH, Yang L, Shimizu K, Pathak JA, Wang H, Wang ZG. J Phys Chem B, in press.
[28] Bhattacharyya AR, Ghosh AK, Misra A, Eichhorn KJ. Polymer 2005;46:1661.
[29] Diaz MF, Barbosa SE, Capiati NJ. Polymer 2007;48:1058.
[30] Ho C-H, Wang C-H, Lin C-I, Lee Y-D. Polymer 2008;49:3902.
[31] Cigana P, Favis BD, Albert C, Vu-Khanh T. Macromolecules 1997;30:4163.
[32] Qiu J, Xu DH, Zhao JC, Niu YH, Wang ZG. J Polym Sci Part B Polym Phys 2008;46:2100.
[33] Muller AJ, Arnal ML, Spinelli AL, Canizales E, Puig CC, Wang H. Macromol Chem Phys 2003;204:1497.
[34] Wang H, Shimizu K, Hobbie EK, Wang ZG, Meredith JC, Karim A, et al. Macromolecules 2002;35:1072.
[35] Cham PM, Lee TH, Marand H. Macromolecules 1994;27:4263.
[36] Inaba N, Sato K, Suzuki S, Hashimoto T. Macromolecules 1986;19:1690.
[37] Inaba N, Yamada T, Suzuki S, Hashimoto T. Macromolecules 1988;21:407.
[38] Hsu CC, Geil PH. Polym Eng Sci 1987;27:1542.
[39] Krishnaswamy RK, Yang Q. Polymer 2007;48:5348.
[40] Tanaka H, Nishi T. Phys Rev Lett 1985;55:1102.